Magazine of Concrete Research: Vol. 40, No. 145: December 1988

Snap-back and hyperstrength in lightly reinforced concrete beams

Alberto Carpinteri

POLYTECHNIC OF TURIN*

SYNOPSIS

The phenomena of hyperstrength and snap-back in lightly reinforced concrete beams are interpreted according to the concepts of fracture mechanics. The tensile strength and toughness of concrete, usually disregarded, are so high in some cases that the maximum bending moment overcomes the bending moment of limit design (hyperstrength). The drop in load capacity hides a virtual softening load–deflection branch with positive slope (snap-back), which can be detected if the loading process is controlled through the crack width.

Notation

A area of concrete
A_s area of steel
a length of crack
B $s_E/\varepsilon_u\lambda$
b slab width or beam depth
E modulus of elasticity
F axial force
f_y yield strength of steel
G_F fracture energy of concrete
h depth of reinforcement
K_I stress-intensity factor
L span
l length of slab
M bending moment
N_p brittleness number (reinforced concrete)
P load
r Equation (20)
s_E brittleness number (plain concrete)
t thickness
w crack width
w_c critical crack width
Y shape functions
δ displacement
ε strain
ε_u ultimate strain
λ slenderness, l/b
ξ relative crack length, a/b
σ tensile stress
σ_u ultimate tensile strength
ϕ rotation

*Department of Structural Engineering, Politecnico di Torino, 10129 Torino, Italy.

Introduction

In this paper the experimental behaviour of lightly reinforced concrete is explained on the basis of simple theoretical models. The unstable fracturing process in reinforced concrete beams as well as the phenomenon of hyperstrength[1] are interpreted according to the principles of fracture mechanics. Such discontinuous behaviour is due to the tensile strength and toughness of concrete, which are usually totally disregarded, but in some cases (e.g. low percentages of reinforcement, high strength of concrete) are so high that the maximum bending moment overcomes the bending moment of limit design. In these cases a drop in the load capacity is predicted by the model[2–4] and verified in practice if the loading process is deflection-controlled.

On the other hand, if the loading process is controlled by the crack width (i.e. the crack width increases smoothly), it is possible to detect a strain-softening load–deflection branch with positive slope. Load and deflection both decrease, while the crack opens and grows in a stable manner. Such a branch is only virtual when the control is achieved by means of the beam deflection. In this case, the crack growth is unstable and a negative jump in the load-carrying capacity of the beam occurs. The catastrophic soften-

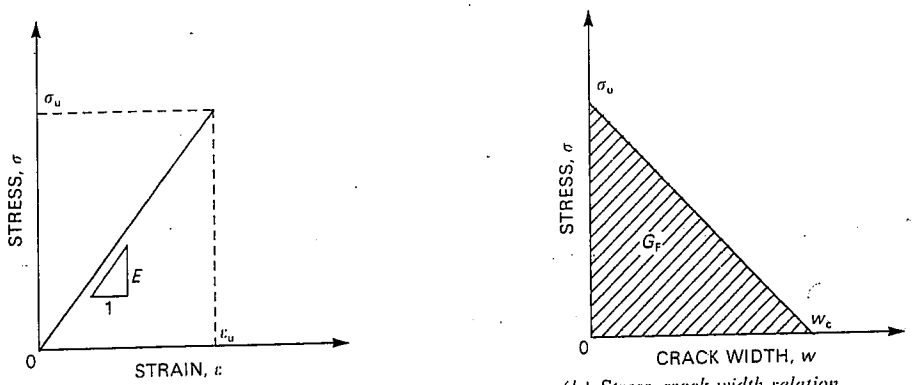

(a) Stress–strain relation *(b) Stress–crack width relation*

Figure 1: Double constitutive law for concrete in tension.

ing branch can be interpreted through a material model with a double constitutive law: linear elastic stress–strain relation, and softening stress–crack width relation[5-7].

Cohesive crack model and catastrophic softening behaviour

Consider an elastic-softening material with a double constitutive law: (1) tensile stress σ–strain ε, and (2) tensile stress σ-crack width w, after reaching the ultimate tensile strength σ_u or strain $\varepsilon_u = \sigma_u/E$ (Figure 1):

$$\sigma = E\varepsilon, \quad \text{for } \varepsilon \leqslant \varepsilon_u \ldots . \text{(1a)}$$

$$\sigma = \sigma_u\left(1 - \frac{w}{w_c}\right), \quad \text{for } w \leqslant w_c \ldots \text{(1b)}$$

$$\sigma = 0, \quad \text{for } w > w_c \ldots \text{(1c)}$$

According to Equation (1c), there is no cohesive interaction between the crack surfaces for widths larger than the critical crack width w_c.

As the load on a plane slab is increased, the deformation undergoes three stages.

(1) The slab behaves elastically without damage or fracture zones, Figure 2(a). The displacement of the upper surface is:

$$\delta = \frac{\sigma}{E} l, \quad \text{for } \varepsilon \leqslant \varepsilon_u \ldots \ldots \ldots \text{(2)}$$

(2) After reaching the ultimate tensile strength σ_u, a crack develops in the weakest section of the slab. Observe that, as the stress field is homogeneous, another cause of inhomogeneity must be assumed for strain localization. The slab behaves elastically only outside the fracture zone, Figure 2(b). The displacement of the upper surface is:

$$\delta = \frac{\sigma}{E} l + w, \quad \text{for } w \leqslant w_c \ldots \ldots \ldots \text{(3)}$$

Recalling Equation (1b), Equation (3) gives:

$$\delta = \frac{\sigma}{E} l + w_c\left(1 - \frac{\sigma}{\sigma_u}\right), \quad \text{for } w \leqslant w_c \ldots \text{(4)}$$

While the fracture zone opens, the elastic zone shrinks at progressively decreasing stresses. At this stage, the loading process will be stable only if it is displacement-controlled; i.e. if the external displacement δ is imposed. But this is only a necessary and not sufficient condition for stability.

(3) When $\delta \geqslant w_c$ the reacting stress σ vanishes, the cohesive forces disappear and the slab is completely separated into two pieces, Figure 2(c).

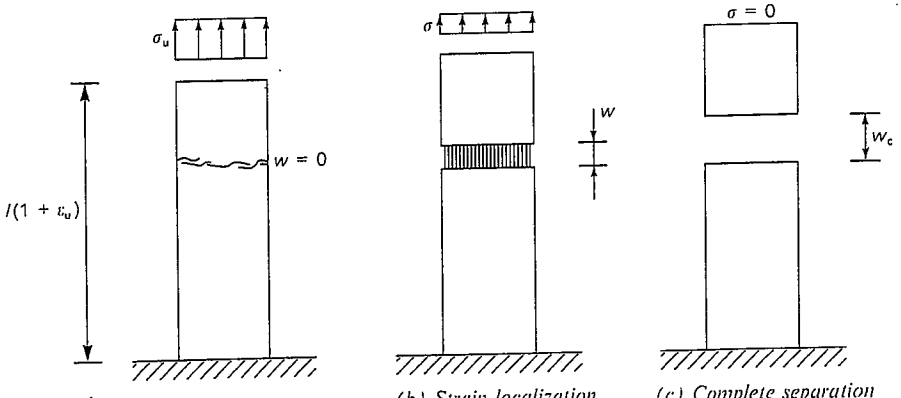

(a) No damage *(b) Strain localization* *(c) Complete separation*

Figure 2: Subsequent stages in the deformation history of a slab in tension.

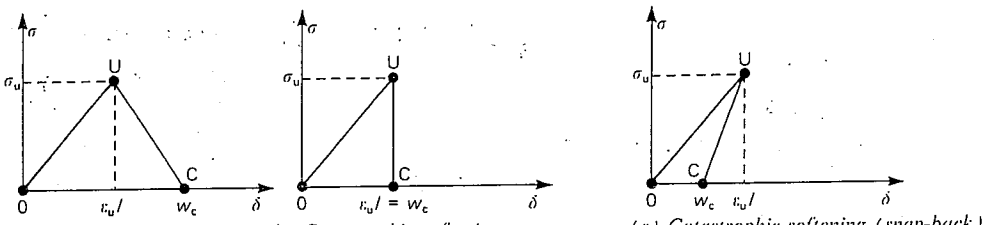

(a) Normal softening (b) Catastrophic softening (c) Catastrophic softening (snap-back)

Figure 3: Stress-displacement response.

Rearranging Equation (2) gives:

$$\sigma = E\frac{\delta}{l}, \quad \text{for } \delta \leqslant \varepsilon_u l \quad \ldots\ldots (5)$$

while the condition of complete separation (stage 3) becomes:

$$\sigma = 0, \quad \text{for } \delta \geqslant w_c \quad \ldots\ldots (6)$$

When $w_c > \varepsilon_u l$, the softening process is stable only if it is displacement-controlled, since the slope $d\sigma/d\delta$ at stage 2 is negative, Figure 3(a). When $w_c = \varepsilon_u l$, the slope $d\sigma/d\delta$ is infinite and a drop in the load capacity occurs, even if the loading is displacement-controlled, Figure 3(b). Eventually, when $w_c < \varepsilon_u l$, the slope $d\sigma/d\delta$ becomes positive, Figure 3(c), and a negative jump occurs like that shown in Figure 3(b).

Rearranging Equation (4):

$$\delta = w_c + \sigma\left(\frac{l}{E} - \frac{w_c}{\sigma_u}\right) \quad \ldots\ldots (7)$$

The same conditions just obtained from a geometrical point of view, Figure 3, may be given also by the analytical derivation of Equation (7).

Normal softening occurs for $d\delta/d\sigma < 0$:

$$\frac{l}{E} - \frac{w_c}{\sigma_u} < 0 \quad \ldots\ldots (8)$$

whereas catastrophical softening occurs for $d\delta/d\sigma \geqslant 0$:

$$\frac{l}{E} - \frac{w_c}{\sigma_u} \geqslant 0 \quad \ldots\ldots (9)$$

Equation (9) may be rearranged:

$$\frac{(w_c/2b)}{\varepsilon_u(l/b)} \leqslant \frac{1}{2} \quad \ldots\ldots (10)$$

where b is the slab width.

The ratio $(w_c/2b)$ is dimensionless and is a function of material properties and structural size[5–7]:

$$s_E = \frac{w_c}{2b} = \frac{G_F}{\sigma_u b} \quad \ldots\ldots (11)$$

$G_F = \frac{1}{2}\sigma_u w_c$ being the fracture energy of the material (Figure 1). The brittleness number s_E describes the scale effects of fracture mechanics, i.e. the ductile–brittle transition when the size-scale is increased. Equation (10) may be presented in the form:

$$\frac{s_E}{\varepsilon_u \lambda} \leqslant \frac{1}{2}, \quad \ldots\ldots (12)$$

where λ = slenderness = l/b.

When the size-scale and the slab slenderness are relatively large and the fracture energy relatively low, the global structural behaviour is brittle. The single values of parameters s_E, ε_u and λ are not responsible for the global brittleness or ductility of the structure considered, but only their combination $B = s_E/\varepsilon_u\lambda$.

When $B \leqslant 1/2$, the plane rectangular slab of Figure 2 shows a mechanical behaviour which can be defined as *brittle* or *catastrophic*. A *bifurcation* or *branching* of the global equilibrium occurs, since, if point U in Figure 3(c) is reached and then the imposed external displacement δ is decreased by a very small amount $d\delta$, the global unloading may occur along two alternative paths: the elastic UO or the virtual softening UC.

The global brittleness of the slab can be defined as the ratio of the ultimate elastic energy contained in the body to the energy dissipated by fracture:

$$\text{Brittleness} = \frac{\frac{1}{2}\frac{\sigma_u^2}{E} \times \text{Area} \times l}{G_F \times \text{Area}} = \frac{1}{2B} \quad \ldots\ldots (13)$$

Such a ratio is higher than unity when Equation (9) is verified and a catastrophic softening instability occurs.

A linear elastic fracture mechanics model for hyperstrength in reinforced concrete beams

Let the cracked concrete beam element in Figure 4 be subjected to a bending moment M and an eccentric axial force F due to the statically indeterminate reaction of the reinforcement. It is well known that bending moment M^* and axial force F^* induce stress-intensity factors at the crack tip:

$$K_I^{(M)} = \frac{M^*}{b^{3/2}t} Y_M(\xi) \quad \ldots\ldots (14a)$$

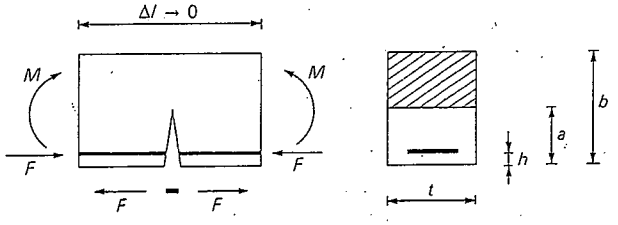

Figure 4: Cracked concrete beam element.

$$K_I^{(F)} = \frac{F^*}{b^{1/2}t} Y_F(\xi) \quad \text{(14b)}$$

where Y_M and Y_F are given in Reference 2.

On the other hand, M^* and F^* produce local rotations:

$$\phi^{(M)} = \lambda_{MM} M^* \quad \text{(15a)}$$

$$\phi^{(F)} = \lambda_{MF} F^* \quad \text{(15b)}$$

where:

$$\lambda_{MM} = \frac{2}{b^2 tE} \int_0^\xi Y_M^2(\xi)\, d\xi \quad \text{(16a)}$$

$$\lambda_{MF} = \frac{2}{btE} \int_0^\xi Y_M(\xi) Y_F(\xi)\, d\xi \quad \text{(16b)}$$

Up to the moment of steel yielding or slippage, the local rotation in the cracked cross-section is assumed to be equal to zero:

$$\phi = \phi^{(M)} + \phi^{(F)} = 0 \quad \text{(17)}$$

Equation (17) is the congruence condition giving the unknown force F. Recalling that, Figure 4,

$$M^* = M - F(b/2 - h) \quad \text{(18a)}$$

$$F^* = -F \quad \text{(18b)}$$

Equations (15) and (17) provide:

$$\frac{Fb}{M} = \frac{1}{(1/2 - h/b) + r(\xi)} \quad \text{(19)}$$

where:

$$r(\xi) = \frac{\int_0^\xi Y_M(\xi) Y_F(\xi)\, d\xi}{\int_0^\xi Y_M^2(\xi)\, d\xi} \quad \text{(20)}$$

If perfectly plastic behaviour of the reinforcement is considered (yielding or slippage), from Equation (19) the moment of plastic deformation for the reinforcement is obtained:

$$M_P = F_P b \left[\left(\frac{1}{2} - \frac{h}{b} \right) + r(\xi) \right] \quad \text{(21)}$$

However, if the concrete has a low compressive strength and the steel a high yield strength, crushing of the concrete can precede plastic deformation of the reinforcement.

The mechanical behaviour of the cracked reinforced concrete beam section is rigid until the bending moment M_P is exceeded, i.e. $\phi = 0$ for $M \leqslant M_P$. On the other hand, for $M > M_P$ the $M(\phi)$ diagram becomes linear-hardening:

$$\phi = \lambda_{MM}(M - M_P) \quad \text{(22)}$$

After plastic deformation of the reinforcement, the stress-intensity factor at the crack tip is given by the superposition principle:

$$K_I = K_I^{(M)} + K_I^{(F)} \quad \text{(23)}$$

Recalling Equation (14) and considering the loadings:

$$M^* = M - F_P(b/2 - h) \quad \text{(24a)}$$

$$F^* = -F_P \quad \text{(24b)}$$

the global stress-intensity factor results:

$$K_I = \frac{Y_M(\xi)}{b^{3/2}t} \left[M - F_P \left(\frac{b}{2} - h \right) \right] - \frac{F_P}{b^{1/2}t} Y_F(\xi) \quad \text{(25)}$$

The moment of crack propagation is then:

$$\frac{M_F}{K_{IC} b^{3/2} t} = \frac{1}{Y_M(\xi)} + N_P \left[\frac{Y_F(\xi)}{Y_M(\xi)} + \frac{1}{2} - \frac{h}{b} \right] \quad \text{(26)}$$

with

$$N_P = \frac{f_y b^{1/2}}{K_{IC}} \cdot \frac{A_s}{A} \quad \text{(27)}$$

while the rotation at crack propagation is:

$$\phi_F = \lambda_{MM}(M_F - M_P) \quad \text{(28)}$$

The crack propagation moment is plotted in Figure 5 as a function of the crack depth ξ and the brittleness number N_P. For low N_P values, i.e. for lightly reinforced beams or for small cross-sections, the fracture moment decreases as the crack extends, and a typical unstable fracture occurs. For $N_P \geqslant 0{\cdot}7$, a stable branch follows the unstable one, while for $N_P \geqslant 8{\cdot}5$ only the stable branch remains. The locus of the minima is represented by a dashed line in Figure 5. In the upper zone the fracture process is stable whereas it is unstable in the lower one.

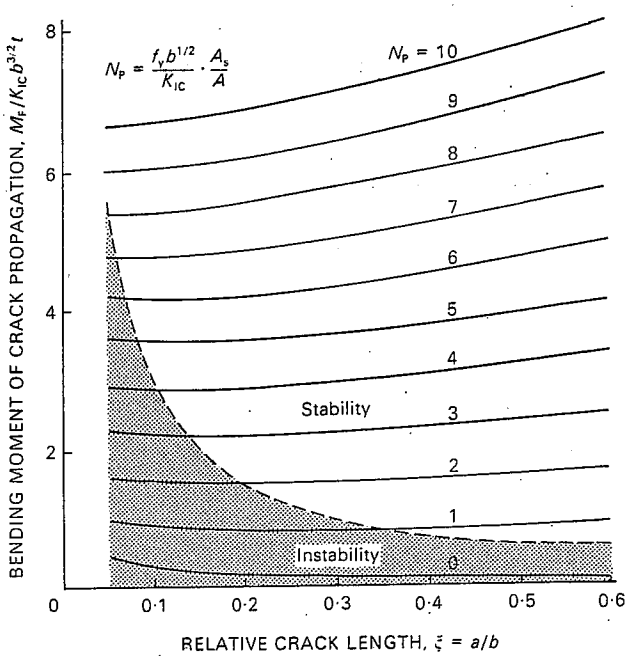

Figure 5: Crack propagation moment versus relative crack length.

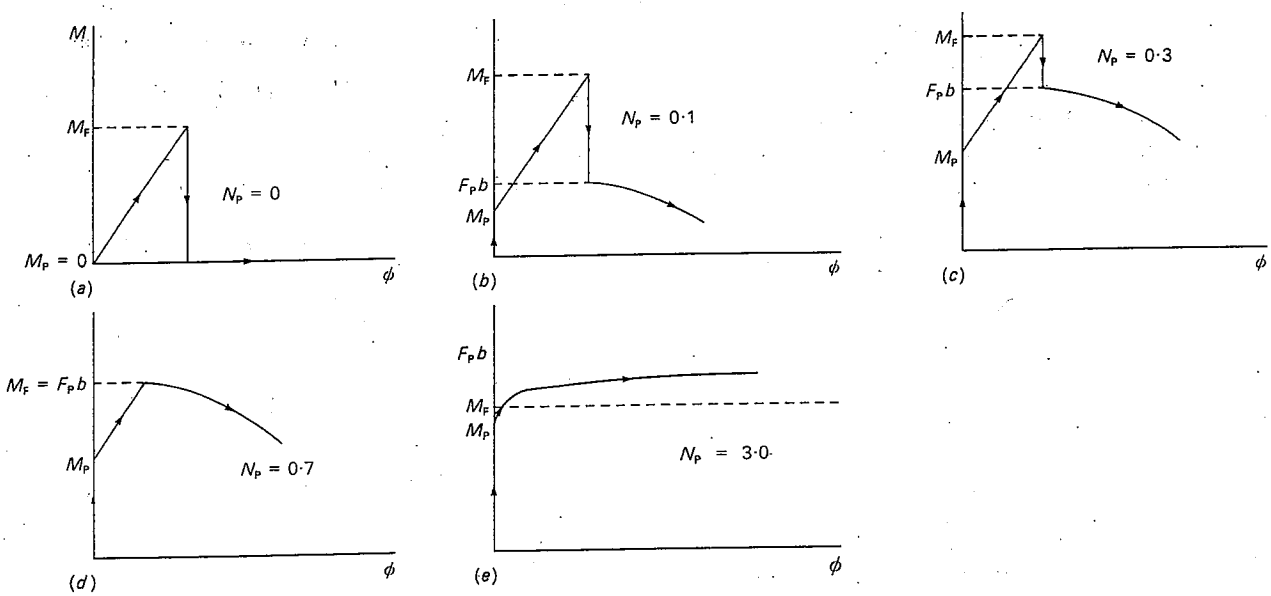

Figure 6: Mechanical behaviour of the cracked reinforced beam section, for different values of the brittleness number $N_P = (f_y b^{1/2}/K_{IC})A_s/A$.

In Figure 6 the moment-rotation diagrams, $M(\phi)$, are reported for $h/b = 1/20$, $\xi = 0{\cdot}1$, and for five different values of brittleness number N_P: 0, 0·1, 0·3, 0·7 and 3·0. Once the cross-section sizes and the mechanical properties of the material have been defined, they represent five different steel areas.

Rigid behaviour ($0 \leqslant M \leqslant M_P$) is followed by linear-hardening behaviour ($M_P < M \leqslant M_F$) which stops when crack propagation occurs. If the fracture phenomenon is unstable, function $M(\phi)$ presents a discontinuity and drops from the value M_F to $F_P b$ with a negative jump, Figures 6(a) to (d). In fact, in this case a complete and instantaneous disconnection of the concrete cross-section occurs. While the rotation, ϕ, is constant, the new moment, $F_P b$, can be estimated according to the scheme of Figure 7, where each beam segment is subjected to the traction, F_P, of the reinforcement and to the contact compression F_P, i.e. altogether, to the moment $F_P(b - h) \simeq F_P b$. Then, increasing the rotation, the bending moment decreases nonlinearly (Figure 7):

$$M = F_P b \cos(\phi/2) \quad \ldots\ldots\ldots (29)$$

On the other hand, if the fracture phenomenon is stable, function $M(\phi)$ does not present any discontinuity and describes hardening behaviour, Figure 6(e).

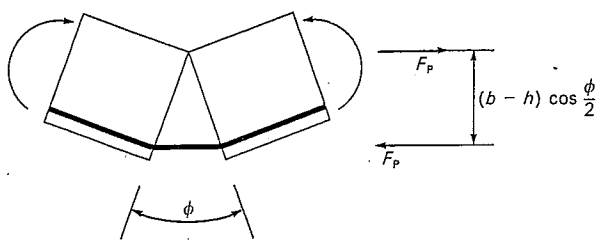

Figure 7: Statical scheme of limit design.

For $N_P \leqslant 0{\cdot}7$, $F_P b \leqslant M_F$, and a discontinuity appears in the $M(\phi)$ diagram, Figures 6(a) to (d), and also the curves in Figure 5 lie completely in the unstable zone. Therefore, it is possible to conclude that, by increasing the steel percentage A_s/A or by increasing the beam size b (A_s/A being constant), the concrete fracturing process becomes stable.

Experimental confirmation of snap-back behaviour

A lightly reinforced concrete beam was tested in flexure by Levi et al.[8]. Load–crack width and load–deflection curves were recorded, Figures 8(a) and (b). The loading process was controlled by the crack width and since this is a monotonically increasing function of time during the fracturing process, it was also possible to detect the *snap-back softening* branch with positive slope of the load–deflection diagram. In this way, a phenomenon unstable in nature was made stable in practice. While load and deflection both decrease between A and B, Figure 8(b), at the same time the crack opens and grows in a stable manner, Figure 8(a). The elementary softening model (Figure 1) can interpret such unstable behaviour completely.

If the loading process had been deflection-controlled, on the other hand, the load-bearing capacity would have shown a negative jump and the catastrophic softening branch would have been only virtual. In this case, the loading drop can be described through the Linear Elastic Fracture Mechanics (LEFM) model (Figure 4). In fact, the high compressive strength of concrete and the small steel area give priority to the steel bar yielding in preference to concrete crushing. In addition, in high strength concrete, the stress-singularity in the crack tip region develops and

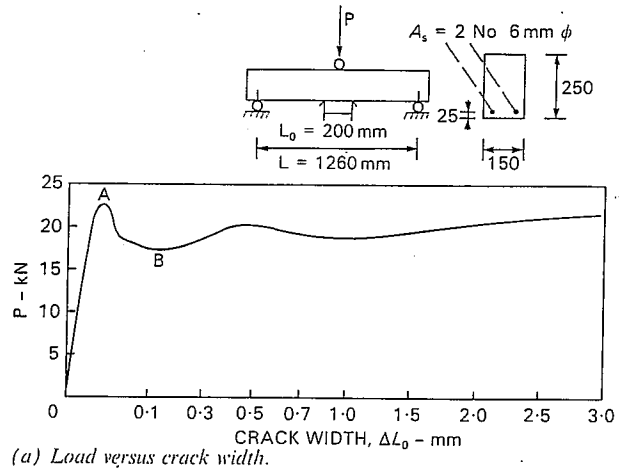

(a) Load versus crack width.

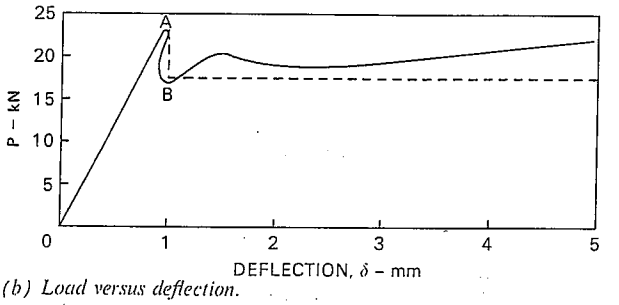

(b) Load versus deflection.

Figure 8: Experimental results from Reference (8).

dominates, which is consistent with the use of LEFM. The apparent *hyperstrength* of concrete is therefore produced by the tensile strength and toughness of this material, which, traditionally, are completely disregarded.

The experimental response is thus predicted by the LEFM model accurately, as the dashed line in Figure 8(b) shows clearly. The geometrical and material features of the specimen provide a dimensionless number $N_P \simeq 0{\cdot}3$, corresponding to the particular case of Figure 6(c) ($b = 250$ mm, $A_s/A = 0{\cdot}15\%$, $f_y \simeq 5000$ kg/cm^2, $K_{IC} \simeq 120$ kg/cm$^{3/2}$).

Experimental confirmation of size effect

Remarkable size-scale effects are theoretically predicted and experimentally confirmed in lightly reinforced high strength concrete beams[9]. The brittleness of the system increases by increasing the beam size and/or decreasing the steel area. On the other hand, physically similar behaviour is revealed in the cases when the non-dimensional number[2,3] N_P is the same.

Thirty reinforced concrete beams were tested, with thickness $t = 150$ mm and with depth $b = 100$ mm (case A), $b = 200$ mm (case B), and $b = 400$ mm (case C), respectively[9]. The span was assumed to be

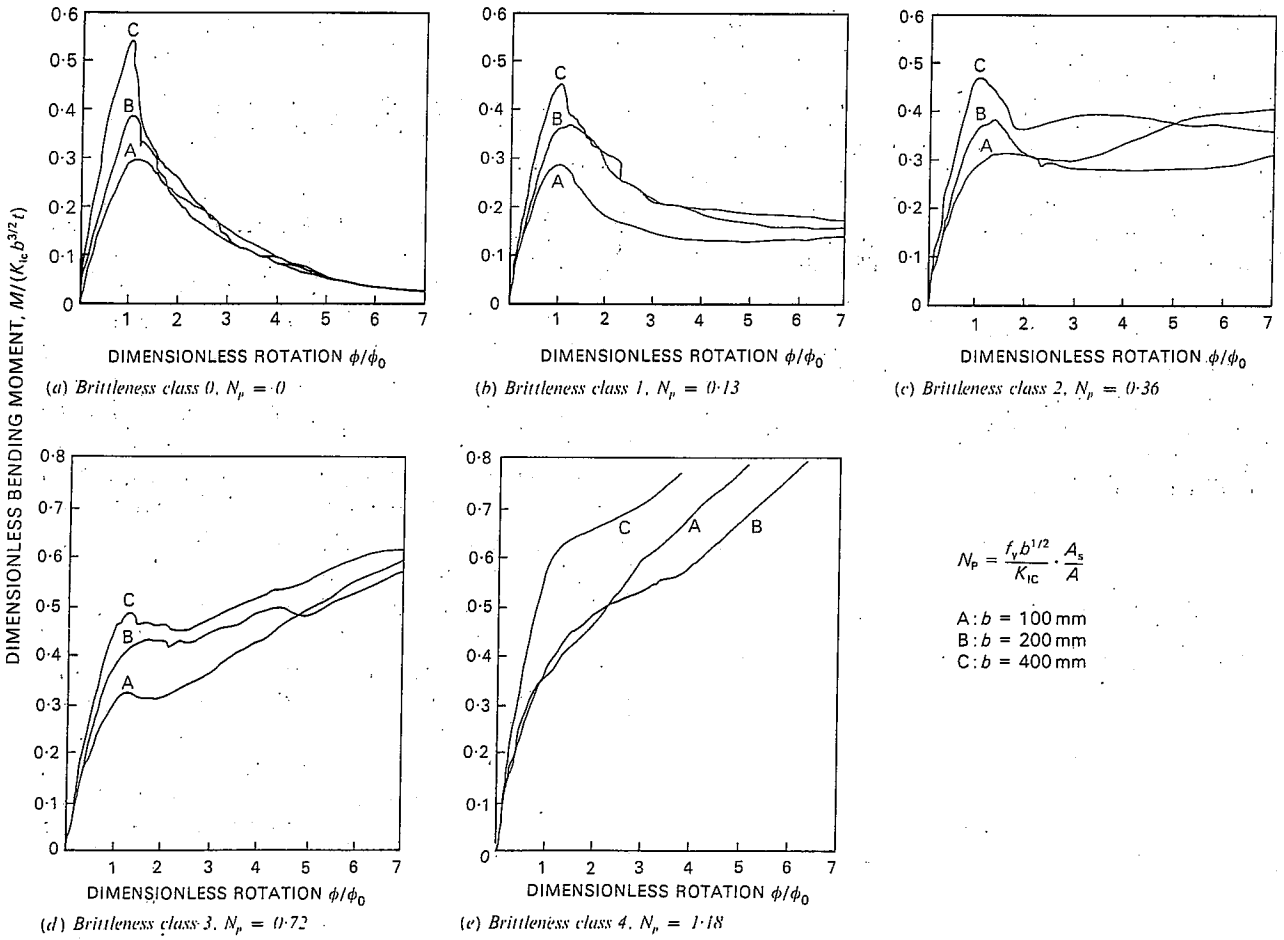

(a) Brittleness class 0, $N_p = 0$ *(b) Brittleness class 1, $N_p = 0{\cdot}13$* *(c) Brittleness class 2, $N_p = 0{\cdot}36$*

(d) Brittleness class 3, $N_p = 0{\cdot}72$ *(e) Brittleness class 4, $N_p = 1{\cdot}18$*

Figure 9: Dimensionless bending moment versus rotation of reinforced concrete beams in flexure, for five different brittleness numbers, N_P[9].

six times the beam depth b. Five different values of N_P were considered (~ 0, 0·10, 0·30, 0·70, 1·20). Both size-scale b and steel percentage A_s/A were varied.

The dimensionless bending moment vs. rotation diagrams are plotted in Figures 9(a) to (e), for each brittleness number N_P and varying beam sizes. The local rotation is referred to the value ϕ_0 of first cracking, and is related to the central beam element of length equal to the beam depth b. The diagrams are significant only for $\phi/\phi_0 > 1$, the strain softening and curvature localization occurring only after the first cracking. The dimensionless peak moment does not appear to be the same, when the brittleness number is the same and the beam depth is varied. This is due to the absence of an initial crack or notch. On the other hand, the post-peak branches are very close to each other and present the same shape for each selected brittleness class.

The LEFM model described in References 2 and 3 is able to capture the most relevant aspects and trends in the mechanical and failure behaviour of lightly reinforced high strength concrete beams in flexure. The extrapolation of predictions from small to large scales is entrusted to the brittleness number N_P, where, in addition to the traditional geometrical and mechanical parameters, even the concrete fracture toughness K_{IC}, or fracture energy G_F, appears.

REFERENCES

1. LEVI, F. On minimum reinforcement in concrete structures, *Journal of Structural Engineering, Proceedings of the American Society of Civil Engineers*. Vol. 111, 1985. pp. 2791–6.
2. CARPINTERI, A. Stability of fracturing process in R.C. beams. *Journal of Structural Engineering. Proceedings of the American Society of Civil Engineers*. Vol. 110, 1984. pp. 544–58.
3. CARPINTERI, A. Hysteretic behaviour of R.C. beams. *Journal of Structural Engineering, Proceedings of the American Society of Civil Engineers*. Vol. 110, 1984. pp. 2073–84.
4. CARPINTERI, A. Scale effects in fracture of plain and reinforced concrete structures. *Fracture Mechanics of Concrete: Structural Application and Numerical Calculation*. Editors: G. C. Sih and A. Di Tommaso. Martinus Nijhoff Publishers, 1985. pp. 95–140.
5. CARPINTERI, A. Interpretation of the Griffith instability as a bifurcation of the global equilibrium. *NATO Advanced Research Workshop on Application of Fracture Mechanics to Cementitious Composites*. Editor: S. P. Shah. Martinus Nijhoff Publishers, 1985. pp. 287–316.
6. CARPINTERI, A., DI TOMMASO, A. and FANELLI, M. Influence of material parameters and geometry on cohesive crack propagation. *Fracture Toughness and Fracture Energy of Concrete*. Editor: F. H. Wittmann. Elsevier Science Publishers, 1986. pp. 117–35.
7. CARPINTERI, A. Limit-analysis for elastic-softening structures: scale and slenderness influence on the global brittleness. *Structure and Crack Propagation in Brittle Matrix Composite Materials*. Editor: A. M. Brandt. Elsevier Applied Science Publishers, 1986. pp. 497–508.
8. LEVI, F., BOSCO, C. and DEBERNARDI, P. G. Two aspects of the behaviour of slightly reinforced structures. *25th CEB-Plenary Session, Treviso, 1987*.
9. BOSCO, C., CARPINTERI, A. and DEBERNARDI, P. G. Fracture of reinforced concrete: scale effects and snap-back instability. *International Conference on Fracture and Damage of Concrete and Rock, Vienna, Austria, July 4–6, 1988*.

Contributions discussing the above paper should be in the hands of the Editor not later than 30 June 1989.